Theoretical investigation of free-standing CoPd nanoclusters as a function of cluster size and stoichiometry in the Pd-rich phase: Geometry, chemical order, magnetism, and metallic behavior

F. Aguilera-Granja and A. Vega
Departamento de Física Teórica, Atómica y Optica, Universidad de Valladolid, E-47011 Valladolid, Spain

José Rogan and X. Andrade
Departamento de Física, Facultad de Ciencias, Universidad de Chile, Casilla 653, Santiago 1, Chile

G. García
Facultad de Física, Universidad Católica de Chile, Casilla 306, Santiago 1, Chile 7820436
(Received 16 May 2006; revised manuscript received 12 October 2006; published 6 December 2006)

We report on a study of the geometrical structure, magnetic properties, and metallic behavior of free-standing CoPd nanoclusters with $N=7$, 13, 19, 23, and 26 atoms, as a function of cluster size and stoichiometry, in the Pd-rich phase. The investigated structures were obtained using a Gupta potential in combination with a genetic algorithm energy minimization. The electronic properties of the ground state geometrical structures were determined by solving a self-consistent *spd* tight-binding Hamiltonian. The metallic behavior was studied using Kubo's criterion. We tested our approach against benchmark SIESTA calculations for some of the small clusters investigated in the present work. We discuss the competition between segregation and mixing effects by means of an order parameter. The magnetic moments are analyzed in the context of the local chemical and atomic environments and we propose a simple empirical expression for the average magnetic moment per atom of these binary clusters.

DOI: 10.1103/PhysRevB.74.224405 PACS number(s): 75.75.+a, 61.46.Bc, 73.22.−f, 36.40.Cg

I. INTRODUCTION

An important goal of the material science nanoengineering design for the following years is the control of the finite size effects, together with the multicomponent character of low-dimensional systems. The nanoalloying design can be very useful from the technological and economical points of view, since it may reduce the cost in the production of active surface nanoparticles, made of very expensive elements, for applications in which inner core atoms do not have to interact with the environment and/or where interactions are just limited to the surface, and also in the context of getting different magnetic properties.[1,2] The nanoalloying design of core/coated arrangements can avoid the use of pure particles of expensive and/or rare elements and reduce the cost of the components. For instance, Pd is an expensive element that is widely used in catalytic processes and frequently appears in its low-dimensional forms, such as clusters and small particles. In order to lower costs, different possibilities have been proposed so that the active Pd component constitutes only a small fraction of the particles. The core/coated configurations can easily be achived in nanometer scale, when segregation takes place in the corresponding bulk alloys, such as in the case of the alloys of Co with all the 4*d* transition metals (TM).[3–6] In other cases the core/coated configurations can be experimentally synthesized, for exmple, in NiPd clusters.[2]

It is expected that controlling both the low-dimensional and the alloying effects, electronic and mechanical properties, not present in bulk systems of both pure and mixed materials, will be found. The first steps in this direction have already been reported in the literature.[1,2,4–9] Many of these investigations, both from the experimental and theoretical viewpoints, are concerned with the low-dimensional effects combined with the alloying in binary clusters made of the 3*d* and 4*d* elements.[1,2,4–7] In such binary nanoclusters, it is expected that the coexistence of the finite size effects and the alloying of a nonmagnetic 4*d* TM with a ferromagnetic 3*d* one could lead to an exotic magnetic scenario. In fact, an example of such magnetic phenomena has been recently reported by Zitoun *et al.*[1] and Nunomura *et al.*[2] for binary nanoparticles of one-hundred atoms synthesized with different atomic configurations for CoRh and NiPd, respectively. In those experiments, an enhancement of the magnetic moment of the binary clusters with respect to the corresponding pure clusters was observed, despite the fact of the nonmagnetic character of the 4*d* elements. Later on, this behavior also was found theoretically.[2,6,7] However, to the best of our knowledge the CoPd nanoclusters have not yet been investigated, neither theoretically nor experimentally. It is the aim of the present paper to report a systematic theoretical study of CoPd nanoclusters in the Pd-rich phase.

It is well-known that both the geometrical structure and the chemical order can play an important role in the magnetism of binary clusters. Therefore, for a correct understanding of the magnetic behavior of the bimetallic nanoclusters it is relevant to investigate the local geometrical and chemical environments within the system, in relation to the local magnetic moments distribution.[4–6] However, in general, the experiments do not provide enough information on the structure and chemical order in the nanoparticles.[1,2] In the present systematic study we have investigated the morphology, the electronic structure, and related properties, like the magnetism and metallicity of CoPd nanoclusters, as a function of cluster size and stoichiometry. The structural properties were investigated via a genetic algorithm on a Gupta potential for

selected sizes (N=7, 13, 19, 23, and 26) for different concentrations in the Pd-rich phase up to the equiatomic concentration. The spin-polarized electronic structure of these clusters has been calculated by solving self-consistently a *spd* tight-binding (TB) Hamiltonian in the mean field approximation, and the metallicity has been studied using Kubo's criterion.[10]

In the following sections we present the theoretical models and approximations used for both the geometric and electronic parts of the problem, together with a benchmark against an *ab initio* density functional theory (DFT) calculation for a CoPd cluster of seven and thirteen atoms. Next, we present and discuss the results and we close the paper with a summary of the main conclusions.

II. THEORETICAL MODEL

The first crucial step in the description and understanding of clusters is the determination of the geometrical structure that the constituent atoms adopt. For the structural search we use a combination of a phenomenological potential, to describe the interactions, and the genetic algorithm as the minimization technique to obtain the minimum energy configurations.

Semiempirical potentials have been used extensively since they were introduced in the mid 1980s. Possibly the first successful attempt is due to Foiles, Baskes, and Daw,[11,12] who put forward the formalism known as the embedded atom method. This formalism was improved upon by Voter and Chen.[13] Other formalisms, different from the embedded atom method, were put forward by Gupta,[14,15] Sutton and Chen,[16] and, more recently, by Murrell and Mottram.[17,18] All of them use many-body potentials, which were fitted to experimental results, like the cohesive energy, lattice parameters, and independent elastic constants for the bulk 0 K crystal structure.

The interatomic interaction between atoms is modeled using the semiempirical Gupta potential. This potential[15] has been derived from Gupta's expression for the cohesive energy of a bulk material[14] and is based on the second moment approximation to TB theory. The Gupta potential has a very simple analytical form which depends on five parameters and is written in terms of repulsive pair and attractive many-body terms, which are obtained by summation over all atoms. The attractive many-body term (the band energy) for atom i is given by

$$E_b^i = -\left[\sum_j \xi_{\alpha\beta}^2 \exp[-2q_{\alpha\beta}(r_{ij}/r_0^{\alpha\beta}-1)]\right]^{1/2}. \quad (1)$$

The stability of the system is ensured by adding a core-repulsion term, of the Born-Mayer type, and given by

$$E_r^i = \sum_j A_{\alpha\beta} \exp[-p_{\alpha\beta}(r_{ij}/r_0^{\alpha\beta}-1)]. \quad (2)$$

In these expressions r_{ij} is the distance between atoms i and j; $\alpha\beta$ stands for CoCo, PdPd, and CoPd; $r_0^{\alpha\beta}$ is the first-neighbor distance in the $\alpha\beta$ lattice; and $A_{\alpha\beta}$, $\xi_{\alpha\beta}$, $p_{\alpha\beta}$, and $q_{\alpha\beta}$ are the potential parameters. For pure elements, the potential parameters are fitted with bulk values of the metals (cohesive energy, the bulk modulus, and the vanishing of the energy gradient at the equilibrium distance).[15] Certainly the use of a potential fitted to bulk properties for computing cluster properties constitutes a first approximation in the absence of specific cluster potentials. For the mixed state, $\alpha\beta$ equal to Co-Pd, the potential parameters were obtained by the geometric mean of the product of the parameters of the pure elements, keeping in mind that it is also a first approximation, an improvement of which would be possible with the availability of the experimental or *ab initio* alloy's heat of mixing for different stoichiometries.

The cohesive energy of the system is given by

$$E_c = \sum_i (E_b^i + E_r^i). \quad (3)$$

We determine the global energy minimum via the genetic algorithm (GA), a search technique based on the principles of natural evolution.[19–21] It uses operators that are analogs of evolutionary processes of mating or crossover, mutation, and natural selection, to explore the multidimensional parameter space. It has been pointed out that the GA is a very efficient approach in locating the optimum cluster structure.[22–24] Using a real valued genome, Zeire[25] calculated the geometry of Ar_nH_2 clusters and found that the average number of evaluations of the cluster potential energy required to reach convergence was less than with a simulated annealing method. In particular, we implemented a GA that uses real numbers (the coordinates for each atoms) in our genome, which makes it necessary to use additional local minimizers within the basin.[26] This combination, GA in real number space and local minimizers, considerably improves the convergence speed, and has proven to be quite reliable.[23,26] With this purpose in mind we implemented two local minimizers: classical simplex and Monte Carlo. Choice of parents is made by the roulette wheel selection method. We also specify the fraction of population that is replaced in each generation and the fraction that remains unchanged (elitism). This kind of GA is know as steady-state GA. To generate a new generation we adopt the following genetic operators: four crossover operators (the arithmetic and geometric means, the N, and the two-point crossover) plus the inversion operator as described by Niesse and Mayne.[26] Additionally, we used a genetic operator that swaps atoms of different species in the binary cluster, in order to analyze its effect on the cluster structure. We also investigated the stoichiometry influence in the final structure by studying a binary cluster of N atoms, with different compositions of Co and Pd. In each case, we performed computations for ten different populations (each of them of 30 individuals). The initial atomic positions were chosen randomly, with the constraint that the average pair separation be between 0.7 and 1.3 of the bulk distance, but smaller than the interaction range. In some cases, we included in the initial populations very few (one or two) selected configurations, based on symmetry properties, to study their feasibility.

The electronic structure of the CoPd nanoclusters, with the morphology determined as explained above, has been calculated by solving a real-space self-consistent *spd* TB Hamiltonian in a mean-field approximation. Notice that self-

consistency is essential in spin-polarized calculations in order to allow for local spin flip processes. In its second quantization form, the Hamiltonian can be written as

$$H = \sum_{i,\alpha,\sigma} \varepsilon_{i\alpha\sigma} n_{i\alpha\sigma} + \sum_{\substack{i,j,\alpha,\beta,\sigma \\ i \neq j}} t_{ij}^{\alpha\beta} c_{i\alpha\sigma}^{\dagger} c_{j\beta\sigma}, \tag{4}$$

where the $t_{ij}^{\alpha\beta}$ stands for the hopping integral for electrons with spin σ between orbitals α and β, at sites i and j, respectively. The density of electrons (the number operator) in the α orbital with spin σ located at site i, is expressed in terms of the creation and annihilation operators, as $n_{i\alpha\sigma}=c_{i\alpha\sigma}^{\dagger}c_{i\alpha\sigma}$. The diagonal elements $\varepsilon_{i\alpha\sigma}$ include the electronic correlations and the spin dependence in the mean-field approximation (see below).

We solved Hamiltonian (4) in a self-consistent way, including hopping integrals up to second neighbors and assuming, as usual, such hopping matrix elements to be spin independent. The chemical dependence of the $t_{ij}^{\alpha\beta}$'s was treated as follows: For the hopping between the same element (Co or Pd), two-center integrals reproducing the metal band structure were used along with the Slater-Koster approximation.[27] For the hopping between Co and Pd atoms, we have used the geometric average of the homoatomic hopping integrals, except for the two-center $pp\pi$ parameter between second neighbors, where an arithmetic mean was used—the parametrization used in Ref. 27 rendered a different sign in the case of Co and Pd.

The changes of the hopping integrals, reflecting in turn the deviation of the interatomic distances from their bulk values, were considered via a power law of the type $(r_0/r_{ij})^{l+l'+1}$. Here r_0 represents the bulk distance, between first or second neighbors, with l and l' standing for the orbital angular momenta of the electronic states involved in the process.[28]

The first term on the right-hand side of Eq. (4) incorporates on the one hand, the spin dependence of the Hamiltonian and, on the other, the electronic correlations (in the mean-field approximation) via a shift of the energy levels of the form

$$\varepsilon_{i\alpha\sigma} = \varepsilon_{i\alpha}^{0} + \frac{1}{2} z_{\sigma} \sum_{\beta} J_{i\alpha\beta} \mu_{i\beta} + \Omega_{i\alpha}, \tag{5}$$

with the bare energy of orbital α at site i, denoted by $\varepsilon_{i\alpha}^{0}$, and the exchange integrals represented by $J_{i\alpha\beta}$. The change in sign of the second term on the right-hand side of Eq. (5), when switching from spin-up to spin-down, is accounted for by the sign function $z_{\sigma}=\pm 1$. The spin polarization of the sp band, due to hybridization with the d states, is negligible as compared with the dominant d band polarization. Thus in our treatment of the spin-dependent part of Hamiltonian (4), we have only considered exchange integrals for the d electrons. Notice, however, that spin-polarization of the delocalized sp band will occur due to hybridization with the d band. In what follows, we have taken the exchange integral associated with Co atoms equal to 1.44 eV, in order to reproduce the fcc Co bulk magnetic moment, without orbital contribution, of $1.59\mu_B$ (Ref. 29). Since palladium metal is paramagnetic, we have taken $J_{dd}=0.50$ eV so that it reproduces the magnetic moments of the Pd_{13} cluster as predicted by first-principles density functional calculations.[30]

In our model, the local electronic occupation is fixed by linear interpolation between the atom and the metal occupations, according to the coordination, at site i. The self-consistent potential $\Omega_{i\alpha}$, the last term in Eq. (5), insures the local proper electronic occupation. Note that $\Omega_{i\alpha}$ has both an orbital and a site dependence. We have used the following electronic configurations for the isolated atoms: Co=[Ar] $3d^7$ $4s^2$ and Pd=[Kr] $4d^9$ $5s^1$. The metal electronic occupations, on the other hand, are those given in Ref. 27: 0.64 (0.60), 0.34 (0.45), and 8.02 (8.95) for the s, p, and d electrons of Co (Pd), respectively. The local charge neutrality approximation has been probed to be a good approximation in TM systems.[31] Our TB model is solved using the recursion method,[28] with a sufficient number of levels in the continued fraction to ensure the stability of the results. As usual, a small imaginary part for the energy is added. This broadens the electronic states facilitating the numerical convergence.

The description of the magnetic properties of low-dimensional $4d$ TM systems requires the same ingredients as for the $3d$ series, in particular, the explicit consideration of the electronic delocalization in order to account for the itinerant character of the magnetism of these materials, and also the particular symmetry of each system which plays an important role due to the directional bonding. The fact that this TB model has been successfully applied to the study of pure Co and Pd clusters[32,33] gives us confidence for the present study of the binary clusters.[4,6] Nevertheless, it is worth testing our approach through a benchmark with a more sophisticated DFT method.

III. RESULTS

A. Tight-binding and DFT results

To the best of our knowledge there are no experimental or *ab initio* reports in the literature for CoPd clusters in the size range considered here. With the aim to check the relability of our calculations we have performed detailed first principles pseudopotential DFT calculations using the SIESTA[34] code (Spanish Initiative for Electronic Simulation of Thousand Atoms) for some selected clusters investigated in the present work, with different sizes, compositions, and/or chemical order. We have chosen small size clusters allowing SIESTA to perform at the same time both the electronic and geometrical calculation with a manageable computational requirement. The results are then compared with those obtained by our combined TB model. We consider Co_2Pd_5, Co_4Pd_9, and Co_6Pd_7. Both Co_2Pd_5 and Co_4Pd_9 have similar Co concentration (≈ 0.3) but different sizes. Co_4Pd_9 and Co_6Pd_7 have the same size but different composition. We have also considered two different chemical orderings for Co_6Pd_7.

SIESTA is a DFT method that employs a linear combination of pseudoatomic orbitals as a basic set. The atomic core is replaced by a nonlocal norm-conserving Troullier-Martins[35] pseudopotential that is factorized in the Kleinman-Bilander form[36] and may include nonlinear terms correcting for the significant overlap of the core charges with

TABLE I. Comparison of the atomic charges and magnetic moments calculated with SIESTA and tight-binding for selected size clusters with different Co concentration.

	$(s+p)_{Pd}$	d_{Pd}	μ_{Pd}	$(s+p)_{Co}$	d_{Co}	μ_{Co}	μ
Co_2Pd_5							
GA-TB	1.01	8.98	0.67	1.51	7.49	2.47	1.18
SIESTA	0.82	9.20	0.63	1.23	7.72	2.34	1.14
Co_4Pd_9							
GA-TB	1.02	8.98	0.45	1.36	7.64	1.97	0.92
SIESTA	0.79	9.26	0.35	1.12	7.76	2.21	0.92
Co_6Pd_7							
GA-TB	1.03	8.98	0.41	1.40	7.59	2.10	1.19
SIESTA	0.78	9.29	0.22	1.09	7.83	2.08	1.08
Co_6Pd_7 isomer							
GA-TB	1.03	8.98	0.26	1.40	7.59	2.02	1.07
SIESTA	0.78	9.29	0.24	1.09	7.83	2.05	1.08

the valence d orbitals. The SIESTA code allows one to perform, together with the electronic calculation, structural optimization in different ways, like conjugate gradients or Verlet algorithm, and it has been successfully applied to a variety of systems like surfaces, adsorbates, nanotubes, biological molecules, and free and supported clusters.

In the present calculation we have used for the exchange and correlation potential the generalized gradient approximation (GGA) of Perdew-Burke-Ernzerhof.[37] The ionic pseudopotentials were generated using the atomic configurations: $4s^1$, $4p^0$, and $3d^8$ for Co and $5s^1$, $5p^0$, and $4d^9$ for Pd with corresponding cutoff radius of 2.30(2.00), 2.46(2.00), and 1.67(2.00) a.u. for Pd (Co). The core corrections are included with core radius of 2.00 and 0.75 a.u. for Pd and Co, respectively. Valence states have been described using double-ζ basis sets with two orbitals having different radial form to describe both the $4s$ $(5s)$ and the $3d$ $(4d)$ shells of Co (Pd) and one orbital to describe the $4p$ $(5p)$ shell. We consider an electronic temperature of 25 meV, and a 350 Ry energy cutoff has been used to define the real space grid for numerical calculations involving the electron density; a larger cutoff does not substantially modify the results. The structural optimization has been carried out by quenching molecular dynamics, using the conjugate gradient algorithm, starting with the geometry obtained from the GA-Gupta calculation.

For Co_2Pd_5, we have a decahedral structure, with the Pd atoms located at the center of the cluster in the pentagonal ring. The SIESTA calculation preserves the decahedral symmetry resulting from our semiempirical model (within a tolerence for the forces of 0.01 eV/Å in the SIESTA calculations). The only difference is that it gives slightly larger interatomic distances ($\approx 6\%$) and a slightly more oblate shape. For the other clusters, with $N=13$ atoms, regardless of the Co/Pd concentration and chemical order the SIESTA calculation also preserves the icosahedral symmetry resulting from our semiempirical model (more details about the structures will be given in the next section). Again, about 6% larger interatomic distances resulted from the SIESTA calculations, which also produce slightly more deformed icosahedra than the semiempirical model. It is expected that deformations are present, particularly at small size clusters. Those deformations are better described in the SIESTA model than in the semiempirical one being fitted to bulk properties. However, it is worth noticing that the interatomic distances provided by SIESTA are closer to the bulk values than the semiempirical ones.

Concerning the electronic and magnetic properties, Table I summarizes the values of the electronic occupations and local and average magnetic moments. In general, the overall qualitative agreement between both theoretical approaches is fairly good, in particular concerning the average magnetic moment, for which a difference of no more than 10% in the absolute values is obtained. A parallel magnetic coupling within the clusters is obtained in both approaches. Larger quantitative differences are obtained for some local magnetic moments in the Co and/or Pd sites. In Co_4Pd_9, the GA-TB model provides larger (lower) local moments in the Pd(Co) sites than SIESTA, but a compensation takes place and the same average magnetic moment results from both approaches. Larger differences are found for the Pd moments of Co_6Pd_7. However, since the Co moments in this cluster are quite similar in both approaches, the resulting average magnetic moment differs only by 10%.

Such differences come, to a large extent, from the different treatments of the charge transfer. Notice that our local neutrality condition prevents charge transfer between the different elements. This can be quantified in Table I by comparing the electronic occupations. Nevertheless, provided that charge transfer is small in TM systems,[31] it does not reflect substantially in the resulting magnetic moments. In the present case the charge transfer between the different elements obtained with the SIESTA model is also negligiable. Concerning the charge transfer between different orbitals, it amounts in general to no more than 0.3 electrons. In the worst case, these 0.3 electrons would imply a maximum error of 0.3 μ_B if all that charge would come from the same

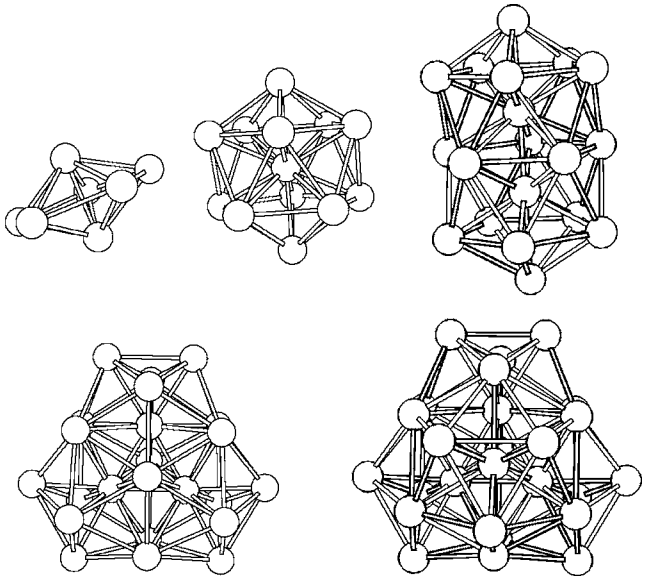

FIG. 1. Ground state structures for CoPd binary clusters resulting from the genetic algorithm for $N=7$, 13, 19, 23, and 26, respectively. For the sake of simplicity we do not distinguish between the different chemical species.

spin-band, which is not generally the case unless the system is magnetically saturated. Therefore these results give further support to our combined GA-TB model. Moreover, it is important to keep in mind that the goal of the present study is to provide qualitative trends, and that for this purpose, with the GA-TB approach one can handle larger clusters than with any DFT approach, being possible to study a larger variety of clusters (different sizes and stoichiometry) with reasonable computer requirements.

B. Structural properties and chemical order

The geometrical structures of the binary clusters, with $N=7$, 13, 19, 23, and 26 atoms, resulting from the minimization process, are illustrated in Fig. 1. An icosahedral-like family of structures is obtained: decahedral ($N=7$), icosahedral ($N=13$), double icosahedral ($N=19$), triple icosahedral ($N=23$), and quadruple icosahedral ($N=26$).

Let us briefly describe how the Co and Pd atoms are distributed within the geometrical structures of Fig. 1. $N=7$ is the only case where we do not have internal atoms in the cluster. We have considered two different concentrations: Co_2Pd_5 and Co_5Pd_2. For Co_2Pd_5 (Co_5Pd_2) the five Pd (Co) atoms are located at the pentagonal ring of the cluster.

For $N=13$, which is the extensively investigated size in free-standing clusters of many elements, we have considered all the relative Co/Co concentrations from Co_1Pd_{12} to Co_7Pd_6 that will serve us later to discuss the trends of the investigated electronic properties as a function of the stoichiometry. The central site is always occupied by a Co atom. Subsequent Co atoms are connected among themselves although not always in a compact way. In general, the segregation competes with the mixing (see Fig. 2) and therefore it will be pertinent to analyze later the balance of both trends as a function of Co concentration.

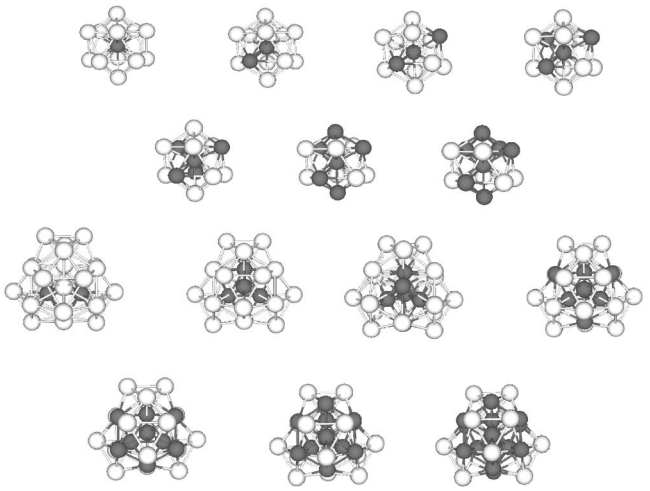

FIG. 2. Illustration of the different geometrical arrays from the genetic algorithm as increasing the Co concentration for $N=13$ and 26. Co atoms are shown with dark balls whereas Pd are the white ones.

Coming now to $N=19$ we have a double icosahedral shape. Here we study Co_2Pd_{17}, Co_7Pd_{12}, and Co_9Pd_{10}. The Co atoms tend to occupy the inner sites. Two Co atoms form a pair at the center, a decahedron is built with seven Co atoms and a double capped decahedron is formed with nine Co atoms in Co_2Pd_{17}, Co_7Pd_{12}, and Co_9Pd_{10}, respectively. For $N=19$, more compact internal Co subclusters are formed than in the $N=13$ case. This fact already motivates us to also analyze the balance of both the mixing and segregation trends as a function of cluster size and not only as a function of stoichiometry (or relative concentration).

For $N=23$ we have a triple icosahedral shape that corresponds to three interpenetrated double icosahedral clusters sharing three internal sites that form an equilateral triangle. We consider Co_3Pd_{20}, Co_5Pd_{18}, Co_9Pd_{14}, $Co_{11}Pd_{12}$, and $Co_{12}Pd_{11}$. The scenario here is similar to that of $N=19$, with Co located in the central part of the cluster. Three Co atoms are located at the center of the cluster forming a triangle, five Co atoms form an hexahedron, nine Co atoms form a symmetrical double capped decaheadron (wedge shape), 11 Co atoms form a fully capped hexahedron, and 12 Co atoms form a four capped decahedron.

Finally, in the case of $N=26$, we have a polyicosahedral cluster formed by four interpenetrated double icosahedral clusters sharing an internal tetrahedral unit. Since in the case of $N=13$ we have considered an extended stoichiometric family, and in order to study in a systematic way the trends of the investigated electronic properties also as a function of the cluster size for a fixed stoichiometry, for $N=26$ we have considered all the relative Co/Pd concentration corresponding to those considered in $N=13$. This is possible by doubling the number of Co and Pd atoms of the $N=13$ clusters and leads to clusters from Co_2Pd_{24} to $Co_{14}Pd_{12}$ with an even number of both Co and Pd atoms. The two internal Co atoms always form a pair, a tetrahedron of Co is built at the center for Co_4Pd_{22} and a capped hexahedron for Co_6Pd_{20}. For larger Co concentration we have a multicapped tetrahedral growth sequence as is illustrated in Fig. 2. The segregation form

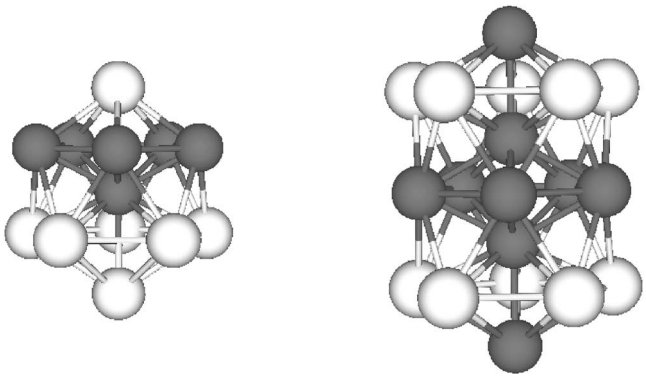

FIG. 3. Illustration of two isomers with layerlike order for $N=13$ and 19, quoted like *isomer* in Table II.

highly symmetric internal Co subclusters at the center of the cluster as for $N=19$ and 23.

Exceptionally, in order to perform a more complete analysis close to the equiatomic concentration, we have taken into account two additional isomers of $N=13$ and 19, Co_6Pd_7 and Co_9Pd_{10}, respectively, that are illustrated in Fig. 3.

Shrinking of the interatomic distances is very common in atomic clusters. In a binary cluster of elements with different bulk lattice constant the reduction in the interatomic distance is due to a combination of the stoichiometry and finite size effects. Thus it is interesting to distinguish the contribution of each effect. A summary of the geometrical properties of the different clusters we studied is presented in Table II. In this table we report the average nearest neighbor distance (ANND) for the different species (Co-Co, Pd-Pd, Co-Pd), the total ANND in the cluster, as well as this value but normalized to the ANND of a hypothetical cluster of the same size with ideal bulk interatomic distances (Δ), and finally the respective multiplicities of the different type of bonds that are used to calculate the chemical order parameter σ discussed below.

The ANND increases with cluster size and decreases with the Co concentration in an almost monotonic way, as expected due to the shorter interatomic distance of the Co fcc bulk relative to the Pd one. The larger the Co concentration the shorter the ANND in the cluster. This trend is clearly illustrated in Fig. 4. The size dependence of the ANND can also be observed in this figure, since for a given Co concentration the largest interatomic distances correspond to the largest clusters in general.

The ANND quantifies the absolute reduction of the cluster volume, thus allowing one to compare it with different clusters, independently of their characteristics. However, each cluster has a binary character with a particular stoichiometry, to quantify its real volume compression requires one to take explicitly into account the relative Co/Pd concentration in the evaluation of the ANND. This can be done by normalizing the ANND of each cluster with respect to the ANND of this same cluster but having ideal bulk interatomic distances. In Fig. 5 we plot the dependence of this quantity (Δ) as a function of Co concentration. We can say that the shrinking, compared with the corresponding hypothetical ideal bulk alloys, goes from $\approx 8\%$ in the case of the smallest clusters to $\approx 4\%$ or less for the largest clusters. The dependence of Δ with Co concentration is very smooth, like the dependence of the ANND, but interesting facts, that justify the analysis of Δ, emerge; for instance, we can say that Co_2Pd_5 really shrinks more than Co_5Pd_2 despite the ANND being smaller for the later one (see also Fig. 4).

To conclude the structural discussion, and with the aim to analyze globally the trend of the chemical order (segregation or mixing) in the different clusters as a function of size and stoichiometry, it is convenient to define an order parameter with the following characteristics: positive when phase-separation (segregation) takes place, close to zero when mixing together with disorder happens, and negative when mixing and layerlike structure coexist. The σ parameter is thus defined as

$$\sigma = \frac{N_{\text{Co-Co}} + N_{\text{Pd-Pd}} - N_{\text{Co-Pd}}}{N_{\text{Co-Co}} + N_{\text{Pd-Pd}} + N_{\text{Co-Pd}}}, \tag{6}$$

where N_{ij} (with i, j=Co, Pd) is the number of nearest-neighbors i-j bonds. The number of these different kinds of bonds corresponds to the multiplicities given in Table II. An order parameter of this sort has proven to be useful in the description of the short-range order in binary bulk alloys and surfaces.[38] The values of σ in our clusters are plotted in Fig. 6. We find that for low Co concentration (lower than 0.2) segregation takes place for all cluster sizes (that is a Co core surrounded by onionlike Pd layers) whereas for larger Co concentrations, small size clusters ($N=7$, 13 in their ground state) exhibit layerlike behavior, but large size ones are mainly chemically disordered with slight segregation character. Notice that for $N=13$ and 19, and close to the equiatomic concentration, we had considered two other isomers (different from the ground state) with a σ-behavior different from the one discussed above for both families of sizes (filled square and diamond in Fig. 6 for $N=13$ and 19, respectively). In this way, having two isomers of the same size, structure, and stoichiometry, but with different chemical order, will help us later to enrich the discussion on the relation between magnetism and chemical order.

C. Magnetic behavior

Let us now present the results obtained for the magnetic properties. In Fig. 7, we plot the average magnetic moment per atom ($\bar{\mu}$) as a function of the Co concentration for all the clusters. As a general trend, we observe the increase of $\bar{\mu}$ with Co concentration, independent of the cluster size. In this respect, it is quite illustrative in Fig. 7 the dependence for $N=13$ (squares) and $N=26$ (down-triangles), for which many different stoichiometries are studied. Of course, this trend is expected due to the considerably larger magnetic moment of Co with respect to Pd. But going into a more detailed analysis, a relevant question still has to be addressed: for a fixed stoichiometry, how does $\bar{\mu}$ depend on cluster size and why? In general, for a fixed concentration in the rich-Pd phase, the larger the cluster the larger $\bar{\mu}$, an exception being $N=7$ for which the Co atoms have a quite large local magnetic moment (in the saturation limit, see Table III), due to their strong surface effects that dominate over other effects. This

TABLE II. Geometrical properties of the clusters studied here. We report the average nearest neighbor distance for the different species (Co-Co, Pd-Pd, Co-Pd) and for the whole cluster, the normalized interatomic distance Δ, and the respective multiplicities of the different types of bonds. The interatomic distances are given in Å.

Type	Co-Co	Pd-Pd	Co-Pd	ANND	Δ	Multiplicity
Decahedral						
Co_2Pd_5	2.39	2.50	2.44	2.46	0.915	(1,5,10)
Co_5Pd_2	2.28	2.80	2.39	2.38	0.926	(5,1,10)
Icosahedral						
$CoPd_{12}$		2.62	2.49	2.59	0.944	(0,30,12)
Co_2Pd_{11}	2.29	2.62	2.49	2.56	0.941	(1,25,16)
Co_3Pd_{10}	2.28	2.61	2.49	2.54	0.939	(2,20,20)
Co_4Pd_9	2.28	2.60	2.49	2.51	0.937	(3,15,24)
Co_5Pd_8	2.29	2.59	2.49	2.49	0.936	(5,11,26)
Co_6Pd_7	2.30	2.59	2.48	2.47	0.934	(8,8,26)
Co_6Pd_7 isomer	2.31	2.61	2.47	2.47	0.934	(10,10,22)
Co_7Pd_6	2.30	2.58	2.48	2.44	0.932	(12,6,24)
Double icosahedral						
Co_2Pd_{17}	2.27	2.64	2.52	2.59	0.948	(1,45,22)
Co_7Pd_{12}	2.34	2.62	2.49	2.49	0.934	(16,20,32)
Co_9Pd_{10}	2.33	2.61	2.49	2.46	0.933	(22,14,32)
Co_9Pd_{10} isomer	2.32	2.58	2.49	2.46	0.933	(18,10,40)
Triple icosahedral						
Co_3Pd_{20}	2.28	2.65	2.52	2.59	0.951	(3,54,30)
Co_5Pd_{18}	2.33	2.64	2.51	2.55	0.945	(9,42,36)
Co_9Pd_{14}	2.33	2.63	2.50	2.49	0.937	(22,23,42)
$Co_{11}Pd_{12}$	2.33	2.61	2.50	2.46	0.935	(30,15,42)
$Co_{12}Pd_{11}$	2.33	2.61	2.50	2.45	0.933	(34,13,40)
Quadruple icosahedral						
Co_2Pd_{24}	2.35	2.69	2.52	2.65	0.966	(1,79,22)
Co_4Pd_{22}	2.30	2.66	2.59	2.59	0.951	(6,60,36)
Co_6Pd_{20}	2.32	2.66	2.51	2.56	0.946	(12,48,42)
Co_8Pd_{18}	2.32	2.64	2.52	2.53	0.942	(18,36,48)
$Co_{10}Pd_{16}$	2.33	2.64	2.51	2.50	0.937	(27,26,48)
$Co_{12}Pd_{14}$	2.33	2.63	2.51	2.47	0.936	(34,20,48)
$Co_{14}Pd_{12}$	2.33	2.61	2.51	2.45	0.934	(42,12,48)

increase of $\bar{\mu}$ as the cluster size increases (illustrated particularly in the 13 vs 26 atom's clusters) is unexpected *a priori*, based on the general and well known trend in transition-metals that predicts an increase of $\bar{\mu}$ as cluster size decreases, as a consequence of the narrowing of the *d*-band associated to the loss of atomic coordination (surface effect). A close inspection of the local average magnetic moments, given in Table III, allows one to understand the above-mentioned unexpected behavior for $\bar{\mu}$. The surface effect is present, of course, in our binary clusters, and it is reflected in the magnetic moment of the Co atoms, as can be deduced from the component-projected magnetic moments given in Table III see particularly the 13 vs 26 families). Thus the Co moments generally increase as the cluster size decreases, for fixed stoichiometry. However, for the binary clusters another important effect coexists with the surface effect, which is the Pd-Co hybridization. This hybridization induces a magnetic moment in the Pd atoms which feel the local magnetic field of their surroundings. This effect is larger for larger clusters with a fixed stoichiometry, since more Co atoms are present and therefore it competes with the surface effect. Thus the magnetic moment of Pd increases as a function of size (see Table III and overcomes the reduction of the Co moments leading to the general increase of $\bar{\mu}$. Of course, it is expected

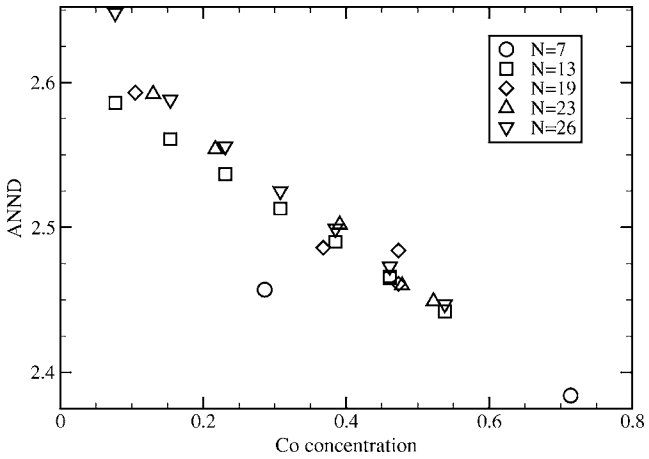

FIG. 4. Average nearest neighbor distance (ANND in Å), as a function of Co concentration, for the different clusters considered here.

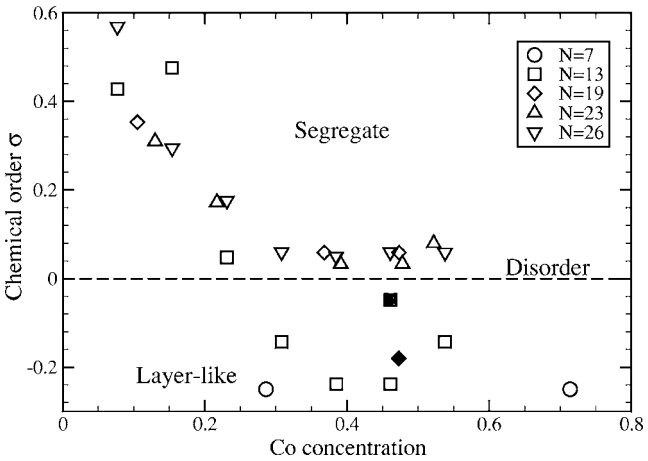

FIG. 6. Chemical order paramater, as a function of Co concentration, for the different clusters as discussed in the text.

that this balance between the surface effect and the hybridization will reverse with a further increase of cluster size, since the reduction of the Co moments will reach a limit (probably the Co bulk value), and at the same time there will be Pd atoms far from the Co sites with very slight or even no induced magnetism. It would be interesting to perform calculations for larger clusters in order to find the critical size for the crossover. Following this argument, one also expects that increasing the Co concentration implies that the surface effects will dominate over the hybridization effect, and this is precisely what we obtain. Look in Fig. 7, how the difference between $\bar{\mu}$ for $N=13$ and 26 is reduced as moving to the Co-rich phase, where it even reverses the trend for a Co concentration of about 0.5. In summary, our results predict an increase of $\bar{\mu}$ as increasing cluster size, for small clusters in the Pd-rich phase.

Both competing effects are implicitly considered by a parameter defined as the ratio $R=\bar{\mu}_{\mathrm{Co}}/\bar{\mu}_{\mathrm{Pd}}$, between the average magnetic moment in Co and the average magnetic moment in Pd, for a given cluster. This ratio R has been studied previously concerning Co/Rh clusters and alloys[1,4,6,39] and it has been found that it depends on the cluster size and stoichiometry. In Fig. 8, we plot R as a function of Co concentration for all the Co/Pd clusters. Let us explain how the magnetic trends discussed previously are reflected in this figure. For a fixed Co concentration in the Pd-rich phase, R is larger for the small clusters than for the big ones, because for the small clusters the surface effect is larger and the hybridization effect is smaller than for the big clusters. These differences are reduced as the Co concentration increases and for a Co concentration of about 0.5, R nearly converges for all sizes. The convergence value (estimated at about 4 and marked with the horizontal line of Fig. 8) is consistent with the value calculated if we consider a Pd impurity in a Co bulk, assuming for Co its fcc bulk moment ($1.6\mu_B$) and for Pd a moment of about 0.4 to $0.5\mu_B$, which is somewhat smaller than our largest calculated moment in Pd to account for the absence of surface effects. The resulting limit of $R\approx 3.5$ is smaller, but notice that the largest clusters here considered are not large enough to be considered as bulk. In the other limit of the Pd-rich phase, R has to dramatically increase due to the nonmagnetic character of Pd bulk. In the

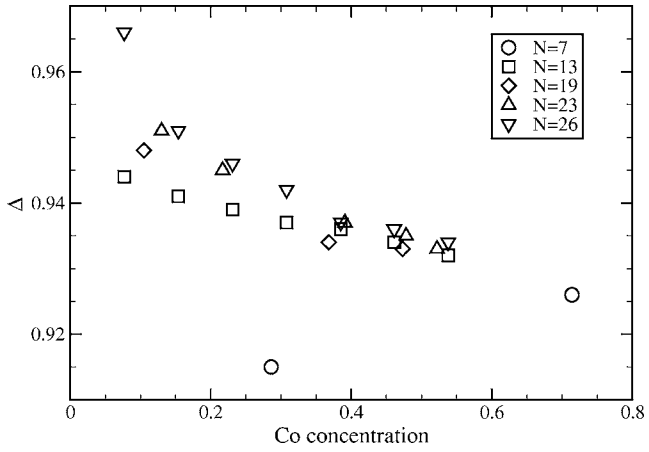

FIG. 5. Δ, as a function of Co concentration, for the different clusters. This paramater give us information on the shrinking suffered by the clusters taking as a reference a hypothetical ideal bulk alloy system.

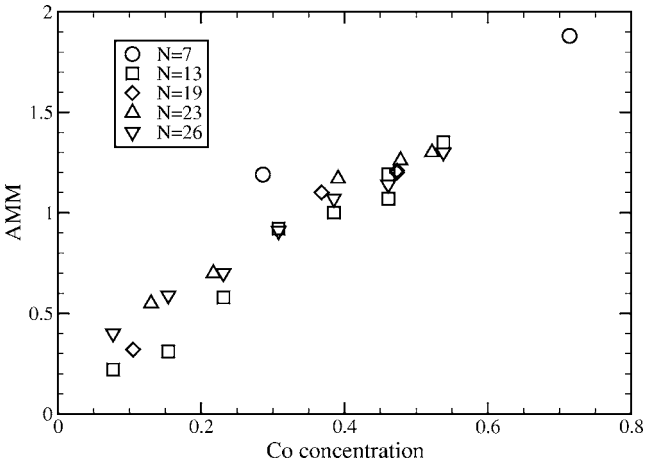

FIG. 7. Average magnetic moment ($\bar{\mu}$), as a function of Co concentration, for the different clusters in units of Bohr magnetons.

TABLE III. Average magnetic moments, $\bar{\mu}$, in units of Bohr magnetons for the clusters considered here and the metallicity temperature (K). In parentheses we give $\bar{\mu}$ calculated using the empirical equation discussed in the text.

Type	$\bar{\mu}$	μ_{Co}	μ_{Pd}	T_M	x(Co)
Decahedral					
Co_2Pd_5	1.19 (1.07)	2.47	0.67	620	0.29
Co_5Pd_2	1.88 (1.85)	2.44	0.48	618	0.71
Icosahedral					
$CoPd_{12}$	0.22 (0.36)	1.48	0.11	286	0.08
Co_2Pd_{11}	0.37 (0.54)	1.72	0.11	352	0.15
Co_3Pd_{10}	0.58 (0.69)	1.91	0.17	361	0.23
Co_4Pd_9	0.92 (0.82)	1.97	0.448	384	0.31
Co_5Pd_8	1.00 (0.94)	2.04	0.348	391	0.39
Co_6Pd_7	1.19 (1.05)	2.10	0.41	351	0.46
Co_6Pd_7	1.07 (1.05)	2.02	0.26	466	0.46
Co_7Pd_6	1.35 (1.15)	2.14	0.420	347	0.54
Double icosahedral					
Co_2Pd_{17}	0.32 (0.45)	1.51	0.18	228	0.11
Co_7Pd_{12}	1.10 (0.95)	1.92	0.61	309	0.37
Co_9Pd_{10}	1.20 (1.10)	1.96	0.52	353	0.47
Co_9Pd_{10}	1.21 (1.10)	1.96	0.53	278	0.47
Triple icosahedral					
Co_3Pd_{20}	0.55 (0.53)	1.60	0.39	194	0.13
Co_5Pd_{18}	0.70 (0.72)	1.74	0.40	232	0.22
Co_9Pd_{14}	1.17 (1.03)	1.93	0.68	265	0.39
$Co_{11}Pd_{12}$	1.26 (1.16)	1.92	0.65	259	0.48
$Co_{12}Pd_{11}$	1.30 (1.22)	1.93	0.61	310	0.52
Quadruple icosahedral					
Co_2Pd_{24}	0.40 (0.40)	1.59	0.30	170	0.08
Co_4Pd_{22}	0.59 (0.61)	1.61	0.41	177	0.15
Co_6Pd_{20}	0.70 (0.77)	1.76	0.37	202	0.23
Co_8Pd_{18}	0.91 (0.92)	1.80	0.52	236	0.31
$Co_{10}Pd_{16}$	1.07 (1.05)	1.84	0.60	254	0.39
$Co_{12}Pd_{14}$	1.14 (1.17)	1.84	0.53	245	0.46
$Co_{14}Pd_{12}$	1.30 (1.28)	1.90	0.62	251	0.54

equiatomic concentration in the bulk limit a value of $R \approx 5.7$ has been experimentally obtained.[40]

Since, as we have seen, $N=7$ is an exceptional case, let us discuss in more detail its magnetic behavior. Here, the magnetic moment of the Co atoms is essentially the same (about $2.4\mu_B$) in the two clusters considered (Co_2Pd_5 and Co_5Pd_2) and, as we have previously pointed out, it is close to the magnetic saturation limit. This is due to the small size of the cluster (notice also that these are clusters without a central site, in contrast to the rest). Although $\bar{\mu}$ of course increases as the Co concentration is increased, the Pd moment is slightly larger (about $0.2\mu_B$) in Co_2Pd_5 than in Co_5Pd_2, in contrast to the discussed trend associated with the Co-Pd hybridization; but one has to keep in mind that symmetry effects also play an important role, in particular for small sizes. In order to understand the local Pd magnetic moments in this case it is necessary to look at the electronic structure. Our model provides both the total and site- and orbital-projected densities of states (DOS). By comparing the paramagnetic DOS at the Pd atoms of the two clusters, we find that in Co_2Pd_5 this Pd DOS displays a larger peak at the Fermi level than in Co_5Pd_2 (about 20% larger). This larger degeneration of Pd states in Co_2Pd_5 with respect to Co_5Pd_2 leads, following the Stoner criterion, to a larger spin-polarization, which is consistent with the larger moment obtained for Pd in the former cluster. In general, deviations

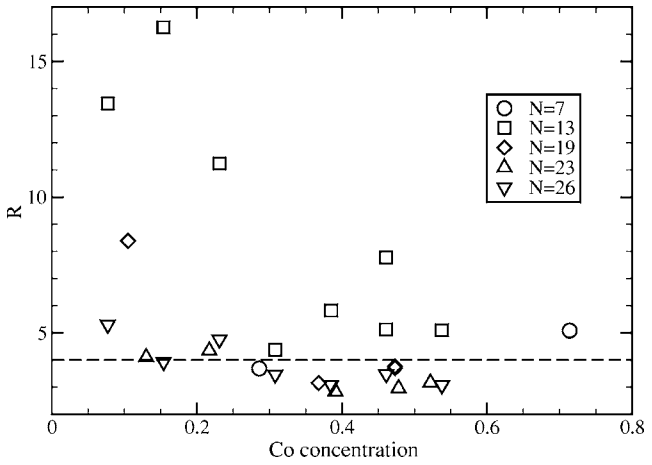

FIG. 8. The $R=\bar{\mu}_{Co}/\bar{\mu}_{Pd}$ ratio, as a function of Co concentration, for the different clusters. The horizontal line estimates the alloy value based on the larger clusters (see text).

from the general trends are associated to particular symmetry effects that are reflected in the electronic structure.

Up to now we have analyzed the magnetic trends as a function of cluster size and stoichiometry; but it remains to discuss the role played by the chemical order. We can shed some light here by comparing, for both $N=13$ and in $N=19$, the ground state configurations with the additional isomer considered (Fig. 3). Fixing size, structure, and stoichiometry, the only free variable is the chemical order. For $N=13$, $\bar{\mu}$ is only about 10% larger in the mixed Co_6Pd_7 cluster than in the segregated one, although the average magnetic moment for the Pd atoms is larger in the mixed cluster than in the segregated one, which is consistent with the larger hybridization when the Co and the Pd atoms are mixed (more average Co coordination for the Pd atoms). For $N=19$ the difference of the average magnetic moments of the segregated and the mixed Co_9Pd_{10} clusters is negligible, although the local magnetic moment for both species are different in the different cluster decorations. Our results indicate that for equiatomic concentrations in the small size regime, the chemical order does not substantially modify the average magnetic properties of the binary clusters. This can be understood taking into consideration that most of the atoms are surfacelike atoms bonded among themselves. Nevertheless, it is expected that in the large size regime this will not be the case, since phase separation will give rise to a substantial part of the system composed by nonpolarized Pd atoms (not bonded with Co), whereas in the mixed situation most of the Pd atoms will have some Co coordination.

It would be interesting to find an empirical expression accounting for the different effects, like the low coordination and hybridization, that play a role in the magnetism of these binary clusters and in terms of which we have tried to understand the trends obtained through the self-consistent TB method. We have found that within our model, in a first approximation, a flat dependence for the average magnetization normalized to the product of the average coordination number (Z) of the clusters times the Co concentration (x_{Co}) to a given power ($\alpha=3/5$) can be obtained for each cluster size. This leads to the following empirical expression for the average magnetization per atom in the cluster of size N:

$$\bar{\mu} \approx ZA(N)x_{Co}^{\alpha}, \tag{7}$$

where $A(N)$ is a size-dependent function that can be fitted to a simple form: $A+B/N^4$ with $A=0.237$ and $B=621.6$. Notice that this empirical expression for $\bar{\mu}$ accounts in a very simple way for the obtained increase of the average magnetization when increasing the atomic coordination and the Co concentration in the Pd-rich phase. In Table III, we report the values obtained using this formula for the different clusters (in parenthesis in the first column), from which the quality of the fit can be inferred. In order to further test the ability of this empirical expression to provide the order of magnitude of the average magnetic moment of Co/Pd clusters in the Pd-rich phase, we performed TB calculations for three clusters that are not included in the fit: Co_1Pd_{78} with cubo-octahedral structure, and Co_1Pd_{54}, $Co_{13}Pd_{42}$ with icosahedral structures. For these clusters we have considered the ANND of the corresponding bulk alloy and we have not done structural optimizations. The average magnetic moments obtained with the self-consistent TB model, $0.14\mu_B$, $0.16\mu_B$, and $0.79\mu_B$, respectively, are very similar to those obtained with the simple empirical expression: $0.15\mu_B$, $0.17\mu_B$, and $0.79\mu_B$, respectively. Although we believe that this expression may be useful to provide an order of magnitude without the need of solving the more sophisticated self-consistent calculation, one has to take care, since the empirical dependence may fail in the limits of the bulk and of the pure clusters, as well as for other $3d$-$4d$ binary clusters.

D. Metallicity

Small clusters of metallic elements are insulators (nonmetallic) due to the discrete distribution of the electronic density of states. A transition from nonmetallic to metallic behavior with increasing cluster size is expected when a band structure is established (or a quasicontinuous electronic distribution) due to the increase of the number of atoms in the system. Kubo and co-workers introduced a simple qualitative theoretical criterion to identify in first approximation this transition,[10] pointing out that it should occur when the average spacing between the electronic levels becomes smaller than k_BT and the discrete energy levels begin to form a quasicontinuous band. In terms of the density of states the transition takes place when the value of the DOS at the Fermi level exceeds $1/k_BT$. Although Kubo's criterion is simple to apply, there are many materials for which this study has not been performed. Some of the authors of the present work successfully used this approximation to study nonmetal-metal transition of pure Ni clusters.[41] The electronic distribution in general depends on the geometrical structure and composition in the case of binary clusters. The former implies that even for a fixed size, some clusters may have more metallic character than others, depending on the composition and also on the chemical order. Of course, Kubo's criterion allows one to derive only a first qualitative insight on the problem, since a deeper understanding would require one to accurately determine the HOMO-LUMO gap and to consider the electronic correlations at finite temperature.

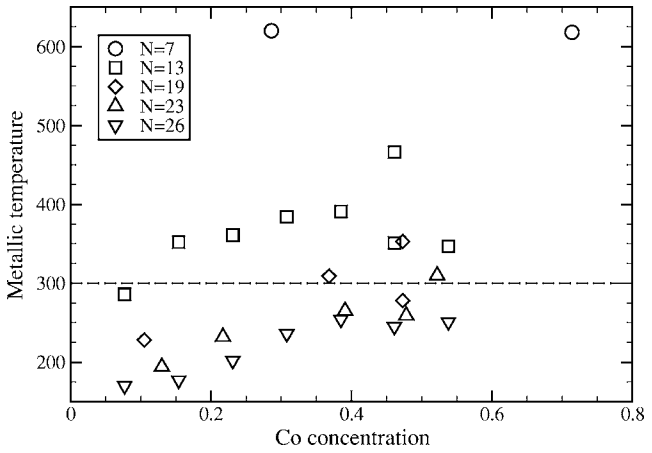

FIG. 9. Metallicity temperature (in K), as a function of Co concentration, for the different clusters. The horizontal line denotes the room temperature.

In Fig. 9, we show the metallic temperature as a function of the Co concentration. This is the temperature above which the cluster starts behaving like a metal. Numerical values are reported in Table III. In general, as expected, our results indicate that the larger the cluster the lower the temperature required for the cluster to become metallic. Moreover, for a fixed size, the metallicity, in general, decreases almost monotonically as the Co concentration increases, so that clusters with larger Pd concentration are more metallic or, in other words, they require lower temperature to behave like a metal. This can be understood by analyzing the total and element-projected densities of states. In general, when increasing the Pd concentration, the highest occupied states become more degenerate and have more Pd character. Notice that this is consistent with the fact that the value of the paramagnetic DOS at Fermi level of Pd bulk largely exceeds the value of the ferromagnetic DOS of Co bulk. In this figure we can also observe that, for a given size and concentration, the metallicity can also change with the chemical order (see $N=13$, 19 closest to the equiatomic concentration). Although for both cases we have found that the segregated clusters have less metallic character than the mixed ones, we cannot generalize this trend without more extensive calculations for other clusters. In Fig. 9 the horizontal line marks the room temperature. Clusters below this line behave in a first approximation, as metallic at room temperature whereas those above are nonmetallic.

IV. SUMMARY AND CONCLUSIONS

Using a genetic algorithm on a Gupta potential and a self-consistent *spd* tight-binding model, we have investigated the morphology, electronic structure, magnetic behavior, and metallicity of CoPd nanoclusters with $N=7$, 13, 19, 23, and 26 atoms, as a function of cluster size and stoichiometry, in the Pd-rich phase.

The main results are the following.

(i) An icosahedral-like family of structures is obtained. The average nearest neighbor distance increases with cluster size and decreases with the Co concentration in an almost monotonic way.

(ii) A competition between segregation and mixing effects takes place. For low Co concentration (lower than 0.2) segregation is found for all cluster sizes whereas for larger Co concentrations, the chemical disorder starts to dominate.

(iii) A clear increase of $\bar{\mu}$ is obtained when increasing the Co concentration, independently of the cluster size.

(iv) For fixed concentration, our results predict an increase of $\bar{\mu}$ when increasing cluster size, for small clusters in the Pd-rich phase.

(v) We propose a simple empirical expression for $\bar{\mu}$ that accounts for its increase as the atomic coordination and Co concentration is increased.

(vi) The temperature required for the cluster to become metallic is found to decrease when increasing the cluster size. For a fixed size, the metallicity, in general, decreases almost monotonically as the Co concentration increases.

The present work is only a first step towards the understanding of the complex electronic and magnetic behavior of these binary nanoclusters. Further insight will be gained through the inclusion of other effects like the spin-orbit coupling, possible noncollinearity effects, and electronic correlations beyond mean field. We hope that our study will stimulate further experimental work to confirm or refute our results.

ACKNOWLEDGMENTS

This work was partially funded by PROMEP-SEP-CA230. Financial support from the Spanish Ministry of Education and Science (Project No. MAT2005-03415) in conjunction with the European regional development funds and from the Junta de Castilla León (Project No. VA068A06) are gratefully acknowledged. F.A.G. acknowledges the Spanish Ministry of Education and Science for a sabbatical Grant SAB-2004-0129. Two of us (J.R. and X.A.) also acknowledge the partial support by the Fondo Nacional de Investigaciones Científicas y Tecnológicas (FONDECYT, Chile) under Grant No. 1030957. Finally, we also acknowledge the critical reading of the paper suggestions by Miguel Kiwi.

[1] D. Zitoun, M. Respaud, M. C. Fromen, M. J. Casanove, P. Lecante, C. Amiens, and B. Chaudret, Phys. Rev. Lett. **89**, 037203 (2002).

[2] N. Nunomura, H. Hori, T. Teranish, M. Miyake, and S. Yamada, Phys. Lett. A **249**, 524 (1998).

[3] See the data base on http://databases.fysik.dtu.dk/hlsDB/hlsDB.php.

[4] A. Díaz-Ortiz, F. Aguilera-Granja, E. O. Berlanga-Ramírez, J. M. Montejano-Carrizales, K. Michaelian, and A. Vega, Physica B **370**, 200 (2005).

[5] T. Sondón and J. Guevara, J. Magn. Magn. Mater. **272–276**, e1247 (2004).
[6] E. O. Berlanga-Ramírez, F. Aguilera-Granja, J. M. Montejano-Carrizales, A. Díaz-Ortiz, K. Michaelian, and A. Vega, Phys. Rev. B **70**, 014410 (2004).
[7] S. Dennler, J. L. Ricardo-Chavez, J. Morillo, and G. M. Pastor, Eur. Phys. J. D **24**, 237 (2003).
[8] R. Ferrando, A. Fortunelli, and G. Rossi, Phys. Rev. B **72**, 085449 (2005).
[9] M. Calleja, C. Rey, M. M. G. Alemany, L. J. Gallego, P. Ordejón, D. Sánchez-Portal, E. Artacho, and J. M. Soler, Phys. Rev. B **60**, 2020 (1999).
[10] R. Kubo, A. Kawabata, and S. Kobayashi, Annu. Rev. Mater. Sci. **49**, 49 (1984).
[11] M. S. Daw and M. I. Baskes, Phys. Rev. B **29**, 6443 (1984).
[12] S. M. Foiles, M. I. Baskes, and M. S. Daw, Phys. Rev. B **33**, 7983 (1986).
[13] A. F. Voter and S. Chen, Mater. Res. Soc. Symp. Proc. **82**, 175 (1987).
[14] R. P. Gupta, Phys. Rev. B **23**, 6265 (1981).
[15] F. Cleri and V. Rosato, Phys. Rev. B **48**, 22 (1993).
[16] A. Sutton and J. Chen, Philos. Mag. Lett. **61**, 139 (1990).
[17] J. N. Murrell and R. Mottram, Mol. Phys. **69**, 571 (1990).
[18] H. Cox, R. L. Johnston, and J. Murrell, J. Solid State Chem. **145**, 571 (1990).
[19] J. Holland, *Adaptation in Natural and Artificial Systems* (University of Michigan Press, Ann Arbor, MI, 1975).
[20] D. E. Goldberg, *Genetic Algorithms in Search, Optimizations & Machine Learning* (Addison-Wesley, Reading, MA, 1989).
[21] M. Mitchell, *An Introduction to Genetic Algorithms* (MIT Press, Cambridge, MA, 1998).
[22] K. Michaelian, Chem. Phys. Lett. **293**, 202 (1998).
[23] Masao Iwamatsu, J. Chem. Phys. **112**, 10976 (2000).
[24] R. S. Judson, Rev. Comput. Chem. **10**, 1 (1997); R. S. Judson, M. E. Colvin, J. C. Meza, A. Huffer, and D. Gutierrez, Int. J. Quantum Chem. **44**, 277 (1992).
[25] Y. Zeiri, Phys. Rev. E **51**, R2769 (1995); Comput. Phys. Commun. **103**, 28 (1997).
[26] J. A. Niesse and H. R. Mayne, J. Chem. Phys. **105**, 4700 (1996).
[27] D. A. Papaconstantopoulos, *Handbook of the Band Structure of Elemental Solids* (Plenum, New York, 1986).
[28] R. Haydock, *Solid State Physics* (Academic Press, London, 1980), Vol. 35, p. 215.
[29] C. Kittel, *Introduction to Solid State Physics*, 7th ed. (Wiley, New York, 1996).
[30] B. V. Reddy, S. N. Khanna, and B. I. Dunlap, Phys. Rev. Lett. **70**, 3323 (1993).
[31] E. Martínez, R. Robles, A. Vega, R. C. Longo, and L. J. Gallego, Eur. Phys. J. D **34**, 51 (2005).
[32] J. L. Rodríguez-López, F. Aguilera-Granja, K. Michaelian, and A. Vega, Phys. Rev. B **67**, 174413 (2003).
[33] F. Aguilera-Granja, J. M. Montejano-Carrizales, and A. Vega, Phys. Lett. A **332**, 107 (2004).
[34] J. M. Soler, E. Artacho, J. D. Gale, A. García, J. Junquera, P. Ordenjon, and D. Sánchez-Portal, J. Phys.: Condens. Matter **14**, 2745 (2002).
[35] N. Troullier and J. L. Martins, Phys. Rev. B **43**, 1993 (1991).
[36] L. Kleinman and D. M. Bylander, Phys. Rev. Lett. **48**, 1425 (1982).
[37] J. P. Perdew, K. Burke, and M. Ernzerhof, Phys. Rev. Lett. **77**, 3865 (1996).
[38] F. Ducastelle, *Cohesion and Structure* (North-Holland, Amsterdam, 1991), Vol. 3.
[39] G. Moraïtis, H. Dreysse, and M. A. Khan, Phys. Rev. B **54**, 7140 (1996).
[40] P. M. Oppeneer, *Handbook of Magnetic Materials* (North-Holland, Amsterdam, 2001), Vol. 13, p. 229.
[41] F. Aguilera-Granja, S. Bouarab, A. Vega, J. A. Alonso, and J. M. Montejano-Carrizales, Solid State Commun. **104**, 635 (1997).